Experimental Demonstration of Stationary Dark-State Polaritons Dressed by Dipole-Dipole Interaction

Bongjune Kim,[1,*] Ko-Tang Chen,[1] Kuei-You Chen,[1] Yu-Shan Chiu,[1] Chia-Yu Hsu,[1] Yi-Hsin Chen,[2] and Ite A. Yu[1,3,†]
[1]*Department of Physics, National Tsing Hua University, Hsinchu 30013, Taiwan*
[2]*Department of Physics, National Sun Yat-sen University, Kaohsiung 80424, Taiwan*
[3]*Center for Quantum Science and Technology, National Tsing Hua University, Hsinchu 30013, Taiwan*

(Received 15 December 2022; accepted 1 September 2023; published 26 September 2023)

Dark-state polaritons (DSPs) based on the effect of electromagnetically induced transparency are bosonic quasiparticles, representing the superpositions of photons and atomic ground-state coherences. It has been proposed that stationary DSPs are governed by the equation of motion closely similar to the Schrödinger equation and can be employed to achieve Bose-Einstein condensation (BEC) with transition temperature orders of magnitude higher than that of the atomic BEC. The stationary-DSP BEC is a three-dimensional system and has a far longer lifetime than the exciton-polariton BEC. In this Letter, we experimentally demonstrated the stationary DSP dressed by the Rydberg-state dipole-dipole interaction (DDI). The DDI-induced phase shift of the stationary DSP was systematically studied. Notably, the experimental data are consistent with the theoretical predictions. The phase shift can be viewed as a consequence of elastic collisions. In terms of thermalization to achieve BEC, the μm^2-size interaction cross section of the DDI can produce a sufficient elastic collision rate for the stationary DSPs. This Letter makes a substantial advancement toward the realization of the stationary-DSP BEC.

DOI: 10.1103/PhysRevLett.131.133001

Diluted atomic gases were the first successful physical systems to reach the Bose-Einstein condensation (BEC) by cooling the bosonic atoms below the transition temperatures [1,2]. In such systems, particle-particle interactions are usually weak, or their scattering lengths are typically much less than mean particle spacings—that is the diluteness. The rapid development of optical microcavities makes it possible to realize exciton-polariton BEC in solid-state systems [3–7]. Concerning the uses of Bose condensates, exciton-polariton BECs are limited to two-dimensional systems and have lifetimes comparable to or shorter than thermalization times.

A unique platform of stationary dark-state polaritons (DSPs) to achieve BEC was proposed in Ref. [8]. Compared with the exciton-polariton BEC system, the stationary-DSP BEC system is three-dimensional and has a much longer lifetime. The DSPs are bosonic particles and represent the superposition of probe photon and atomic coherence. They are formed by the interaction between a weak probe pulse and atoms under the presence of a strong coupling field based on the effect of electromagnetically induced transparency (EIT) as depicted in Fig. 1(a). The EIT mechanism can store the DSPs in the atoms by turning off the coupling field, and later retrieve the DSPs by turning on the coupling field. Furthermore, when the two counterpropagating coupling fields are applied, the DSPs become stationary and diffuse in the forward and backward directions [9–16].

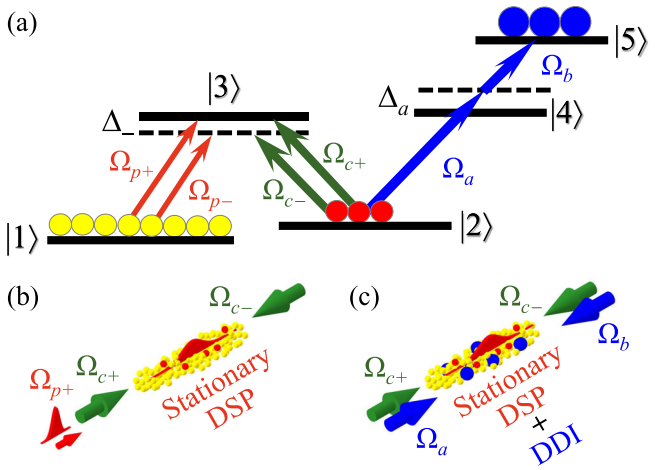

FIG. 1. (a) Relevant energy levels and laser excitations. States $|1\rangle$, $|2\rangle$, and $|3\rangle$ form the Λ-type EIT system for the creation of stationary DSPs, where $\Omega_{p\pm}$ and $\Omega_{c\pm}$ denote the Rabi frequencies of the forward-backward probe and coupling fields, respectively, and $\Delta_- = -1\Gamma$. Population oscillates between $|2\rangle$ and a Rydberg state $|5\rangle$, driven by the TPT of the fields Ω_a and Ω_b with $\Delta_a = +5\Gamma$, where $|4\rangle$ is an intermediate state of the TPT. The spontaneous decay rates of $|3\rangle$ and $|4\rangle$ are about the same and denoted as Γ ($= 2\pi \times 6$ MHz). In this Letter, the pair of Ω_{c+} and Ω_{p+}, that of Ω_{c-} and Ω_{p-}, and that of Ω_a and Ω_b always maintained the two-photon resonances. (b),(c) Propagation directions of the laser fields in the measurements of stationary DSPs without and with the TPT or equivalently the DDI.

In Ref. [8], Fleischhauer *et al.* showed that the stationary DSPs are governed by the equation of motion closely similar to the Schrödinger equation. They further proposed utilizing a nonlinear Kerr effect to mediate the interaction between the DSPs for thermalization to achieve BEC. However, the proposed Kerr-type interaction is typically too weak to make a sufficient elastic collision rate for thermalization. Therefore, this present work aimed to substitute the dipole-dipole interaction (DDI) between Rydberg-state atoms for the Kerr-type interaction to make the stationary-DSP BEC feasible.

Rydberg atoms possess strong DDI [17–21], leading to the applications such as quantum logic gates [22–26], single-photon sources [27–29], and strongly correlated many-body physics [30–33]. In our earlier work, we experimentally demonstrated a many-body system of Rydberg polaritons based on the EIT effect [34], where the Rydberg polariton represents the superposition of the photon and the coherence between a Rydberg and a ground state. Slow light arising from the EIT effect greatly enhances the interaction time between light and matter, which can be a couple of μs to about 10 μs in a medium of high optical depth (OD) [11,34–36]. In the thermalization process, the high-OD medium made the interaction time compatible with the elastic collision rate of the μm^2-size interaction cross section due to the DDI between Rydberg polaritons. Hence, we observed a cooling effect in the transverse direction of slowly propagating Rydberg polaritons [34].

According to Ref. [34], one could create stationary Rydberg polaritons to achieve BEC. The formation of stationary polaritons involves the four-wave mixing (FWM) process [9–16]. The ladder-type transition scheme, which typically has a very large phase mismatch in the FWM process, is employed in the Rydberg-EIT system to form the stationary Rydberg polaritons. However, the probe and coupling fields had the typical wavelengths of 780 or 795 nm and around 480 nm in a Rydberg-EIT system, resulting in an FWM phase mismatch of 10^4–10^5 rad. Such a large phase mismatch completely destroys stationary Rydberg polaritons and makes the search for the Rydberg-polariton BEC impractical.

In this study, we proposed and experimentally demonstrated the stationary DSPs possessing the Rydberg-state DDI. In addition to the probe and coupling fields that formed the stationary DSP via the FWM process, two more laser fields were applied to drive the two-photon transition (TPT) of $|2\rangle \rightarrow |4\rangle \rightarrow |5\rangle$ as shown by Fig. 1(a). The TPT generated the Rabi oscillation between the population of the ground state $|2\rangle$ and that of the Rydberg state $|5\rangle$, as well as between the ground-state coherence ρ_{21} and the Rydberg coherence ρ_{51}. Owing to the existence of the Rydberg population, the DDI resulted in the phase shift and attenuation of the stationary DSP. With regard to the thermalization of stationary DSPs, the DDI can lead to a far larger elastic collision rate than the Kerr-type interaction. Hence, this Letter makes a substantial advancement toward the realization of the stationary-DSP BEC.

We carried out the experiment in laser-cooled ^{87}Rb atoms with a temperature of about 350 μK. Before each measurement, the magnetic and laser fields for the production of the cold atoms were switched off, and we optically pumped all the population to a single Zeeman state. Details of the atom cloud and the experimental procedure before the measurements can be found in Refs. [34,37].

All the laser fields had the σ_+ polarization in the experiment. In the Λ-type EIT system shown by Fig. 1(a), $|1\rangle$, $|2\rangle$, and $|3\rangle$ are $|5S_{1/2}, F=1, m_F=1\rangle$, $|5S_{1/2}, F=2, m_F=1\rangle$, and $|5P_{3/2}, F=2, m_F=2\rangle$. The EIT was driven resonantly, while the fields in the forward direction (Ω_{p+} and Ω_{c+}) had nearly zero one-photon detuning, and those in the backward direction (Ω_{p-} and Ω_{c-}) had the one-photon detuning Δ_- of -1Γ [10]. In the TPT system shown by Fig. 1(a), $|4\rangle$ is $|5P_{3/2}, F=3, m_F=2\rangle$ and $|5\rangle$ is $|32D_{5/2}, m_J=3/2$ and $5/2\rangle$. We made the TPT resonant at nearly no DDI and set the one-photon detuning Δ_a to $+5\Gamma$ to make excitation to $|4\rangle$ negligible.

The propagation direction of Ω_{c-} was exactly opposite to that of Ω_{c+} as depicted in Fig. 1(b). When interacting with the atoms, Ω_{c+} and Ω_{p+} propagated in the nearly same direction with an angle separation of about 0.3° [10]. The backward probe field Ω_{p-}, or more precisely $\Omega_{p-}(z,t)$, depicted in Fig. 1(a) only appeared during the stationary DSP, and its value was nearly the same as $\Omega_{p+}(z,t)$ [10]. Driving the transitions of $|2\rangle \rightarrow |4\rangle$ and $|4\rangle \rightarrow |5\rangle$, the TPT fields with Rabi frequencies of Ω_a and Ω_b counterpropagated in the forward and backward directions as depicted in Fig. 1(c). The laser beams of Ω_a and Ω_b completely covered the region of stationary DSPs. Other details of the experimental setup can be found in Sec. I of the Supplemental Material [38].

We made theoretical predictions using the optical Bloch equations of the density-matrix operator and the Maxwell-Schrödinger equations of the probe fields. Details of the equations and calculation can be found in Sec. II of the Supplemental Material [38]. In our earlier works [41,42], the predictions are in good agreement with the experimental data.

We set $\delta_\Lambda = 0$ in the experiment, where δ_Λ is the two-photon detuning in the Λ-type EIT system. In Ref. [43], Tebben *et al.* theoretically studied a similar transition scheme, except that the TPT is replaced by a one-photon transition. They showed that the optimum δ_Λ, which maximizes the stationary-DSP energy, is equal to a half of the Rabi frequency of the one-photon transition [44]. In our TPT case, $\delta_\Lambda = 0$ is the optimum value.

Representative data that demonstrate the formation of stationary DSPs in the Λ-type EIT system are shown by Fig. 2(a) [Fig. 2(b)] without (with) the TPT. The Rabi oscillation between the population in $|2\rangle$ and that in $|5\rangle$

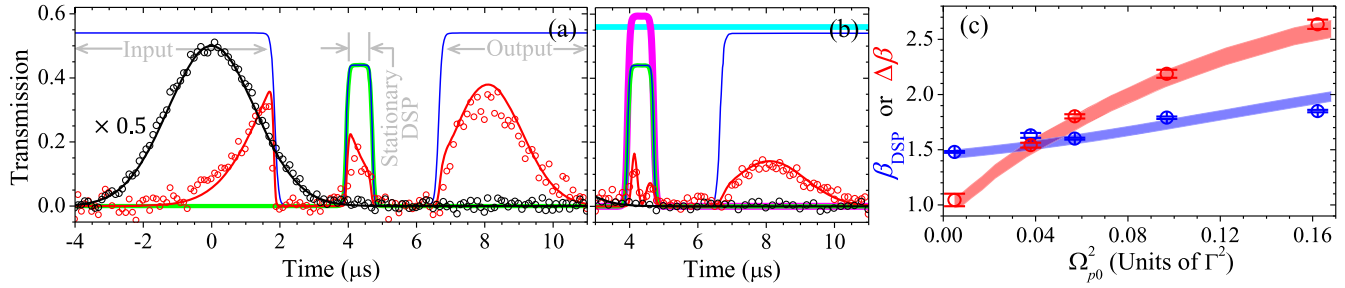

FIG. 2. (a),(b) Representative data demonstrate the consistency with predictions. The analysis of data and the illustration of parameters can be found in text and in Sec. III of the Supplemental Material [38]. Black and red circles are the data of the input and output probe pulses in the forward direction. Black line is the Gaussian best fit of the input probe pulse, and red lines are the predictions of the output probe pulses. Blue, green, magenta, and cyan lines represent the timing sequences of the forward and backward coupling fields Ω_{c+} and Ω_{c-} and the TPT fields Ω_a and Ω_b. We do not plot the data before $t < 3$ μs in (b), which are the same as those in (a). The peak Rabi frequency of the input probe pulse, Ω_{p0}, is 0.07Γ. The experimental parameters of the stationary DSP are α (optical depth) $= 36$, $\Omega_{c+} = 0.54\Gamma$ during the input and output stages, $\Omega_{c+} = \Omega_{c-} = 0.44\Gamma$ and $\Omega_a = \Omega_b = 0$ during the stationary DSP, γ_Λ (the ground-state decoherence rate) $= 9 \times 10^{-4}\Gamma$, and $L\Delta_k$ (the degree of phase mismatch) $= 0.90$ rad; those of the TPT and DDI are $\Omega_a = 2.0\Gamma$, $\Omega_b = 1.6\Gamma$, γ_R (the Rydberg-state decoherence rate) $= 0.020\Gamma$, and A (the DDI coefficient) $= 0.60\Gamma$. (c) The DDI-induced attenuation increased with the Rydberg-state population or equivalently the input probe intensity. The attenuation coefficient (i.e., the logarithm of the ratio of input to output probe energies) without the TPT, β_{DSP}, and the difference between the attenuation coefficients with and without the TPT, $\Delta\beta$ ($\equiv\beta_{DSP+DDI} - \beta_{DSP}$), as functions of Ω_{p0}^2. Blue and red circles are the data of β_{DSP} and $\Delta\beta$, respectively. Based on the above-mentioned parameters, blue and red areas are the predictions with the uncertainties due to the fluctuation of ± 1 in α and that of $\pm 1 \times 10^{-4}\Gamma$ in γ_Λ.

(or between coherences ρ_{21} and ρ_{51}) was clearly observed during the magenta pulse in Fig. 2(b). The consistency between the data and the predictions is satisfactory. More details of the data are described in Sec. III of the Supplemental Material [38].

In the measurements of the DSPs without and with the TPT such as Fig. 2, the Rabi frequencies Ω_{c+}, Ω_{c-}, and Ω_a, the OD (α), and the ground-state decoherence rate (γ_Λ) were predetermined [37,45,46], where the probe transmission without the EIT is indicated by $\exp(-\alpha)$ and the decay rate of the coherence ρ_{21} is represented by γ_Λ. Details of the determination methods and representative data are presented in Secs. I and IV of the Supplemental Material [38]. The Rabi frequency Ω_b was determined by the period of the Rabi oscillation during the TPT. The stationary DSP is generated by the FWM process, in which the phase mismatch causes the energy loss [11,47,48]. The degree of phase mismatch is given by $L\Delta_k$ [see Eq. (S18) in the Supplemental Material [38]]. We determined the value of $L\Delta_k$ by the comparison between the experimental results and theoretical predictions. Details can be found in Sec. V of the Supplemental Material [38], which provides more evidence for the formation of stationary DSPs.

We varied the input probe power [38], while keeping the pulse width and beam profile the same, and measured the data similar to those in Figs. 2(a) and 2(b). The population in $|2\rangle$, ρ_{22}, is about equal to $|\Omega_{p+}/\Omega_{c+}|^2$ due to the EIT effect. Thus, a larger input probe intensity, Ω_{p0}^2, resulted in larger ρ_{22} and ρ_{55}, which produced a higher DDI strength [34]. We determined the attenuation coefficients, β_{DSP} and $\beta_{DSP+DDI}$, as functions of Ω_{p0}^2, where β_{DSP} and $\beta_{DSP+DDI}$ are defined as the logarithm of the ratio of input to output probe energies without and with the DDI, and Ω_{p0}^2 is the square of the Rabi frequency of the input probe pulse peak. In Fig. 2(c), the blue and red circles represent the data of β_{DSP} and $\Delta\beta$ ($\equiv\beta_{DSP+DDI} - \beta_{DSP}$). Since the OD fluctuated about ± 1 and the ground-state decoherence rate γ_Λ fluctuated about $\pm 1 \times 10^{-4}\Gamma$, the predictions of β_{DSP} and $\Delta\beta$ are plotted as the blue and red areas.

The TPT made the population (coherence) oscillate between $|2\rangle$ and $|5\rangle$ (between ρ_{21} and ρ_{51}), and the population in $|5\rangle$ induced the DDI. We characterized the DDI coefficient, A, which is defined as the decoherence rate (also frequency shift) per ρ_{55} [34,41,42]. See also Eqs. (S15) and (S16) in the Supplemental Material [38] for the definition of A. The ratio of retrieved probe energies with and without the TPT was measured against the input probe intensity or equivalently the peak Rabi frequency square, Ω_{p0}^2, as shown in Fig. 2(c). We compared the data with the predictions to determine $A = 0.60\Gamma$ and γ_R (the decay rate of the coherence ρ_{51}) $= 0.020\Gamma$. We also estimated the value of A, and details can be found in Sec. VI of the Supplemental Material [38]. The estimation gives A of 0.54Γ, indicating that the experimentally determined A of 0.60Γ is reasonable.

The DDI induces a phase shift of the stationary DSP, and the phase of the retrieved probe pulse is shifted. To further verify the creation of the stationary DSP dressed by the DDI, we applied the TPT and measured the phase shift of the retrieved probe pulse, i.e., the difference of the phases with and without the atoms. The beat-note interferometer was employed to measure the phase evolution around the

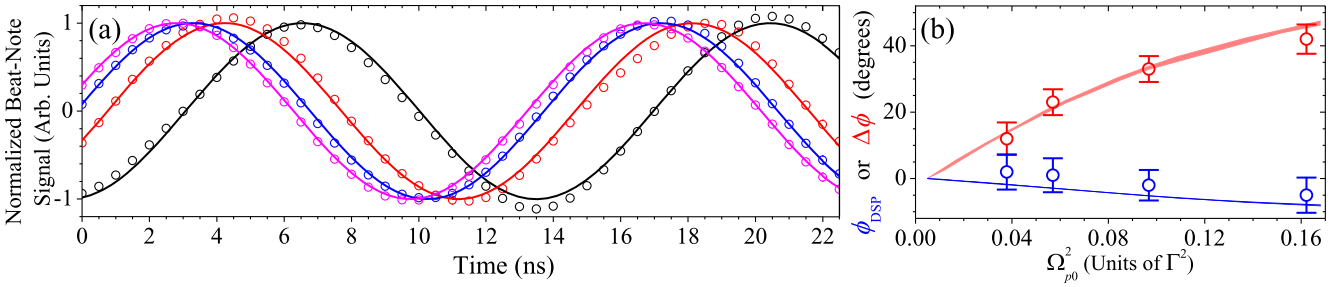

FIG. 3. We show quantitatively that the DDI-induced phase shift during the TPT increased with the Rydberg-state population or equivalently the input probe intensity. The analysis of data can be found in text. (a) Representative data of normalized beat-note signals, showing phase evolutions at the peaks of the retrieved probe pulses. Circles are the experimental data, and lines are their best fits. In the presence of the TPT (or equivalently the DDI) during the stationary DSP, red, blue, and magenta colors correspond to the peak Rabi frequency of the input probe, Ω_{p0}, of 0.07Γ, 0.24Γ, and 0.40Γ, respectively. The beat-note signals of each Ω_{p0} in the absence of the TPT were measured, which serve as the reference phases. We make these three signals completely overlap and plot only one here (black color). The experimental parameters are the same as those specified in the caption of Fig. 2. Since the DDI is negligible at $\Omega_{p0} = 0.07\Gamma$, the phase difference between the red and black data is mainly the result of the Rabi oscillation. On the other hand, the phase difference of $+42°$ (or $+23°$) between the magenta (or blue) and red data is the consequence of the DDI. (b) Blue circles are the data of phase shift of the output probe pulse without the TPT, ϕ_{DSP}, and red circles are those of the difference between the phase shifts with and without the TPT, $\Delta\phi$ ($\equiv\phi_{\mathrm{DSP+DDI}} - \phi_{\mathrm{DSP}}$). The phase shifts at $\Omega_{p0} = 0.07\Gamma$ are subtracted from the data. Blue and red areas are the predictions with the uncertainties due to the fluctuations of α and γ_Λ.

pulse peak [34,49]. The experimental parameters in the phase measurement are the same as those in the transmission measurement. In Fig. 3(a), the black circles are the beat-note data without the TPT or DDI, which serve as the reference for the other data. The red, blue, and magenta circles represent the data with increasing values of Ω_{p0}^2 or DDI strength. A larger DDI strength resulted in a larger phase shift as expected.

We measured the phase shifts of the retrieved probe pulses without and with the TPT, ϕ_{DSP} and $\phi_{\mathrm{DSP+DDI}}$, respectively, as functions of Ω_{p0}^2. In Fig. 3(b), the blue and red circles represent ϕ_{DSP} and $\Delta\phi$ ($\equiv\phi_{\mathrm{DSP+DDI}} - \phi_{\mathrm{DSP}}$). We subtracted the measured phase shift at $\Omega_{p0} = 0.07\Gamma$ from the data. The subtraction removes the phase shift contributed from the Rabi oscillation. Thus, $\Delta\phi$ exhibits mainly the DDI effect. More details can be found in Sec. VIII of the Supplemental Material [38]. Without the DDI, ϕ_{DSP} of the stationary DSP depends on the probe intensity a little. Owing to the DDI, $\Delta\phi$ depends on the probe intensity significantly. The blue and red areas are the theoretical predictions. In the theoretical calculation, all the parameters are nonadjustable and experimentally predetermined. The consistency between the data and predictions is satisfactory, confirming that the stationary DSP indeed possessed the DDI.

As another evidence of the stationary DSPs carrying the DDI, we measured the DDI effect at different Rydberg states $|nD_{5/2}\rangle$ with the principal quantum numbers, n, of 28, 30, 32, 35, and 38. The DDI potential energy between two Rydberg atoms is given by C_6/r^6, where C_6 is the Van der Waals coefficient and r is the distance between the atoms. The DDI energy shift or DDI-induced attenuation coefficient is linearly proportional to $\sqrt{C_6}$ [42,50–52]. In Fig. 4, we plot the experimental data of the DDI-induced attenuation coefficient, $\Delta\beta_{\mathrm{DDI}}$, against $\sqrt{C_6}$, where $\Delta\beta_{\mathrm{DDI}}$ is the difference between the DDI-induced attenuation coefficient of $\Omega_{p0} = 0.24\Gamma$ and that of $\Omega_{p0} = 0.07\Gamma$. This $\Delta\beta_{\mathrm{DDI}}$ can avoid any attenuation effect that depends on n, e.g., different two-photon frequency fluctuations due to different n's, except the DDI effect. The values of C_6 were obtained from the programming code provided by Ref. [53]. The experimental data of $\Delta\beta_{\mathrm{DDI}}$ clearly exhibit the linear dependence on $\sqrt{C_6}$, further confirming that the stationary DSPs possess the DDI.

We now estimate whether the present experimental condition is close to the observation of stationary-DSP BEC. Details of the estimations can be found in Sec. IX of the Supplemental Material [38]. Based on the formulas in Ref. [8], the BEC transition temperature, T_c, is about

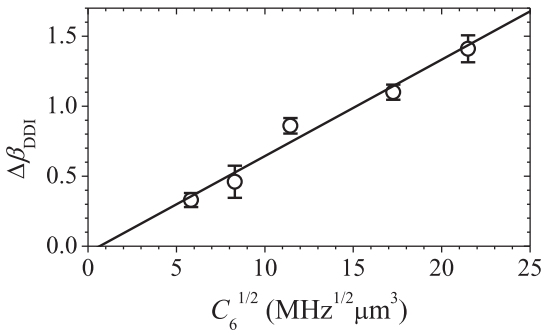

FIG. 4. To further verify that the stationary DSPs carry the DDI, we plot $\Delta\beta_{\mathrm{DDI}}$ against $\sqrt{C_6}$, where $\Delta\beta_{\mathrm{DDI}}$ is the attenuation coefficient depending only on the DDI strength (see the illustration in text) and C_6 is the Van der Waals coefficient [53]. Circles are the experimental data and straight line is the best fit.

4.0 mK, and the stationary-DSP temperature, T_p, is around 3.8 μK. The measured phase shift indicates that the elastic collision rate, R_c, is approximately 33 μs^{-1}. Under $T_p \ll T_c$, such R_c enables the thermal equilibrium of stationary DSPs, and makes the BEC feasible. To observe the BEC, we still need to build an artificial trap and produce stationary DSPs in the quasicontinuous mode.

In conclusion, we experimentally demonstrated the formation of the stationary DSP dressed by the DDI, using the scheme of the Λ-type EIT system together with the TPT-driven Rabi oscillation between a ground state and a Rydberg state. The scheme overcomes the severe problem of a large phase mismatch in the direct formation of the stationary Rydberg polariton. As proposed in Ref. [8], the system of stationary DSPs is the possible platform for a three-dimensional and long-lifetime Bose condensate. Our Letter made the stationary DSPs carry the DDI and provided a feasible method of thermalization for the realization of BEC.

This work was supported by Grants No. 110-2639-M-007-001-ASP and No. 111-2639-M-007-001-ASP of the National Science and Technology Council, Taiwan, and Grant No. 111-2923-M-008-004-MY3 of the Mutual Funds for Scientific Cooperation between Taiwan, Latvia, and Lithuania. The authors are thankful for the fruitful discussions with Prof. Gediminas Juzeliūnas and Mr. Chin-Jen Yang.

*upfe11@gmail.com
†yu@phys.nthu.edu.tw

[1] M. H. Anderson, J. R. Ensher, M. R. Matthews, C. E. Wieman, and E. A. Cornell, Observation of Bose-Einstein condensation in a dilute atomic vapor, Science **269**, 198 (1995).
[2] K. B. Davis, M.-O. Mewes, M. R. Andrews, N. J. van Druten, D. S. Durfee, D. M. Kurn, and W. Ketterle, Bose-Einstein Condensation in a Gas of Sodium Atoms, Phys. Rev. Lett. **75**, 3969 (1995).
[3] J. Kasprzak, M. Richard, S. Kundermann, A. Baas, P. Jeambrun, J. M. J. Keeling, F. M. Marchetti, M. H. Szymańska, R. André, J. L. Staehli, V. Savona, P. B. Littlewood, B. Deveaud, and Le Si Dang, Bose-Einstein condensation of exciton polaritons, Nature (London) **443**, 409 (2006).
[4] H. Deng, H. Haug, and Y. Yamamoto, Exciton-polariton Bose-Einstein condensation, Rev. Mod. Phys. **82**, 1489 (2010).
[5] H. Deng, D. Press, S. Götzinger, G. S. Solomon, R. Hey, K. H. Ploog, and Y. Yamamoto, Quantum Degenerate Exciton-Polaritons in Thermal Equilibrium, Phys. Rev. Lett. **97**, 146402 (2006).
[6] Y. Sun, P. Wen, Y. Yoon, G. Liu, M. Steger, L. N. Pfeiffer, K. West, D. W. Snoke, and K. A. Nelson, Bose-Einstein Condensation of Long-Lifetime Polaritons in Thermal Equilibrium, Phys. Rev. Lett. **118**, 016602 (2017); **118**, 149901(E) (2017).
[7] V. Y. Shishkov, E. S. Andrianov, A. V. Zasedatelev, P. G. Lagoudakis, and Y. E. Lozovik, Exact Analytical Solution for the Density Matrix of a Nonequilibrium Polariton Bose-Einstein Condensate, Phys. Rev. Lett. **128**, 065301 (2022).
[8] M. Fleischhauer, J. Otterbach, and R. G. Unanyan, Bose-Einstein Condensation of Stationary-Light Polaritons, Phys. Rev. Lett. **101**, 163601 (2008).
[9] M. Bajcsy, A. S. Zibrov, and M. D. Lukin, Stationary pulses of light in an atomic medium, Nature (London) **426**, 638 (2003).
[10] Y.-W. Lin, W.-T. Liao, T. Peters, H.-C. Chou, J.-S. Wang, H.-W. Cho, P.-C. Kuan, and I. A. Yu, Stationary Light Pulses in Cold Atomic Media and without Bragg Gratings, Phys. Rev. Lett. **102**, 213601 (2009).
[11] Y.-H. Chen, M.-J. Lee, W. Hung, Y.-C. Chen, Y.-F. Chen, and I. A. Yu, Demonstration of the Interaction between Two Stopped Light Pulses, Phys. Rev. Lett. **108**, 173603 (2012).
[12] F. Blatt, L. S. Simeonov, T. Halfmann, and T. Peters, Stationary light pulses and narrowband light storage in a laser-cooled ensemble loaded into a hollow-core fiber, Phys. Rev. A **94**, 043833 (2016).
[13] G. T. Campbell, Y.-W. Cho, J. Su, J. Everett, N. Robins, P. K. Lam, and B. Buchler, Direct imaging of slow, stored and stationary EIT polaritons, Quantum Sci. Technol. **2**, 034010 (2017).
[14] K.-K. Park, Y.-W. Cho, Y.-T. Chough, and Y.-H. Kim, Experimental Demonstration of Quantum Stationary Light Pulses in an Atomic Ensemble, Phys. Rev. X **8**, 021016 (2018).
[15] J. L. Everett, D. B. Higginbottom, G. T. Campbell, P. K. Lam, and B. C. Buchler, Stationary light in atomic media, Adv. Quantum Technol. **2**, 1800100 (2019).
[16] U.-S. Kim, Y. S. Ihn, C.-H. Lee, and Y.-H. Kim, Trapping a free-propagating single-photon into an atomic ensemble as a quantum stationary light pulse, AVS Quantum Sci. **4**, 021403 (2022).
[17] M. D. Lukin, M. Fleischhauer, R. Cote, L. M. Duan, D. Jaksch, J. I. Cirac, and P. Zoller, Dipole Blockade and Quantum Information Processing in Mesoscopic Atomic Ensembles, Phys. Rev. Lett. **87**, 037901 (2001).
[18] D. Tong, S. M. Farooqi, J. Stanojevic, S. Krishnan, Y. P. Zhang, R. Côté, E. E. Eyler, and P. L. Gould, Local Blockade of Rydberg Excitation in an Ultracold Gas, Phys. Rev. Lett. **93**, 063001 (2004).
[19] R. Heidemann, U. Raitzsch, V. Bendkowsky, B. Butscher, R. Löw, L. Santos, and T. Pfau, Evidence for Coherent Collective Rydberg Excitation in the Strong Blockade Regime, Phys. Rev. Lett. **99**, 163601 (2007).
[20] M. Saffman, T. G. Walker, and K. Mølmer, Quantum information with Rydberg atoms, Rev. Mod. Phys. **82**, 2313 (2010).
[21] J. D. Pritchard, D. Maxwell, A. Gauguet, K. J. Weatherill, M. P. A. Jones, and C. S. Adams, Cooperative Atom-Light Interaction in a Blockaded Rydberg Ensemble, Phys. Rev. Lett. **105**, 193603 (2010).
[22] M. Saffman and T. G. Walker, Analysis of a quantum logic device based on dipole-dipole interactions of optically trapped Rydberg atoms, Phys. Rev. A **72**, 022347 (2005).

[23] T. Keating, R. L. Cook, A. M. Hankin, Y.-Y. Jau, G. W. Biedermann, and I. H. Deutsch, Robust quantum logic in neutral atoms via adiabatic Rydberg dressing, Phys. Rev. A **91**, 012337 (2015).
[24] D. Tiarks, S. Schmidt-Eberle, T. Stolz, G. Rempe, and S. Dürr, A photon-photon quantum gate based on Rydberg interactions, Nat. Phys. **15**, 124 (2019).
[25] J. Vaneecloo, S. Garcia, and A. Ourjoumtsev, Intracavity Rydberg Superatom for Optical Quantum Engineering: Coherent Control, Single-Shot Detection, and Optical π Phase Shift, Phys. Rev. X **12**, 021034 (2022).
[26] T. Stolz, H. Hegels, M. Winter, B. Röhr, Y.-F. Hsiao, L. Husel, G. Rempe, and S. Dürr, Quantum-Logic Gate between Two Optical Photons with an Average Efficiency above 40%, Phys. Rev. X **12**, 021035 (2022).
[27] F. Ripka, H. Kübler, R. Löw, and T. Pfau, A room-temperature single-photon source based on strongly interacting Rydberg atoms, Science **362**, 446 (2018).
[28] D. P. Ornelas-Huerta, A. N. Craddock, E. A. Goldschmidt, A. J. Hachtel, Y. Wang, P. Bienias, A. V. Gorshkov, S. L. Rolston, and J. V. Porto, On-demand indistinguishable single photons from an efficient and pure source based on a Rydberg ensemble, Optica **7**, 813 (2020).
[29] S. Shi, B. Xu, K. Zhang, G.-S. Ye, D.-S. Xiang, Y. Liu, J. Wang, D. Su, and L. Li, High-fidelity photonic quantum logic gate based on near-optimal Rydberg single-photon source, Nat. Commun. **13**, 4454 (2022).
[30] G. Pupillo, A. Micheli, M. Boninsegni, I. Lesanovsky, and P. Zoller, Strongly Correlated Gases of Rydberg-Dressed Atoms: Quantum and Classical Dynamics, Phys. Rev. Lett. **104**, 223002 (2010).
[31] T. Peyronel, O. Firstenberg, Q.-Y. Liang, S. Hofferberth, A. V. Gorshkov, T. Pohl, M. D. Lukin, and V. Vuletić, Quantum nonlinear optics with single photons enabled by strongly interacting atoms, Nature (London) **488**, 57 (2012).
[32] M. Moos, M. Höning, R. Unanyan, and M. Fleischhauer, Many-body physics of Rydberg dark-state polaritons in the strongly interacting regime, Phys. Rev. A **92**, 053846 (2015).
[33] A. Browaeys and T. Lahaye, Many-body physics with individually controlled Rydberg atoms, Nat. Phys. **16**, 132 (2020).
[34] B. Kim, K.-T. Chen, S.-S. Hsiao, S.-Y. Wang, K.-B. Li, J. Ruseckas, G. Juzeliūnas, T. Kirova, M. Auzinsh, Y.-C. Chen, Y.-F. Chen, and I. A. Yu, A weakly-interacting many-body system of Rydberg polaritons based on electromagnetically induced transparency, Commun. Phys. **4**, 101 (2021).
[35] Y.-H. Chen, M.-J. Lee, I.-C. Wang, S. Du, Y.-F. Chen, Y.-C. Chen, and I. A. Yu, Coherent Optical Memory with High Storage Efficiency and Large Fractional Delay, Phys. Rev. Lett. **110**, 083601 (2013).
[36] Y.-S. Wang, K.-B. Li, C.-F. Chang, T.-W. Lin, J.-Q. Li, S.-S. Hsiao, J.-M. Chen, Y.-H. Lai, Y.-C. Chen, Y.-F. Chen, C.-S. Chuu, and I. A. Yu, Temporally-ultralong biphotons with a linewidth of 50 kHz, APL Photonics **7**, 126102 (2022).
[37] B. Kim, K.-T. Chen, C.-Y. Hsu, S.-S. Hsiao, Y.-C. Tseng, C.-Y. Lee, S.-L. Liang, Y.-H. Lai, J. Ruseckas, G. Juzeliūnas, and I. A. Yu, Effect of laser-frequency fluctuation on the decay rate of Rydberg coherence, Phys. Rev. A **100**, 013815 (2019).
[38] See Supplemental Material at http://link.aps.org/supplemental/10.1103/PhysRevLett.131.133001, which includes Refs. [39,40] for the details of the experimental data and theoretical predictions at $\Omega_{p0} \geq 0.3\Gamma$.
[39] S. Chandrasekhar, Stochastic problems in physics and astronomy, Rev. Mod. Phys. **15**, 1 (1943).
[40] W.-T. Liao, T. Peters, E.-C. Shen, and I. A. Yu, Propagation, broadening, and energy decay of quasi-stationary light pulses in thermal atoms, Chin. J. Phys. **47**, 043603 (2009).
[41] K.-T. Chen, B. Kim, C.-C. Su, S.-S. Hsiao, S.-J. Huang, W.-T. Liao, and I. A. Yu, Increasing the decoherence rate of Rydberg polaritons due to accumulating dark Rydberg atoms, Phys. Rev. Res. **4**, 023024 (2022).
[42] S.-S. Hsiao, K.-T. Chen, and I. A. Yu, Mean field theory of weakly-interacting Rydberg polaritons in the EIT system based on the nearest-neighbor distribution, Opt. Express **28**, 28414 (2020).
[43] A. Tebben, C. Hainaut, A. Salzinger, T. Franz, S. Geier, G. Zürn, and M. Weidemüller, A stationary Rydberg polariton, arXiv:2108.00657.
[44] Y.-C. Chen, Y.-A. Liao, H.-Y. Chiu, J.-J. Su, and I. A. Yu, Observation of the quantum interference phenomenon induced by interacting dark resonances, Phys. Rev. A **64**, 053806 (2001).
[45] C.-Y. Wang, Y.-F. Chen, S.-C. Lin, W.-H. Lin, P.-C. Kuan, and I. A. Yu, Low-light-level all-optical switching, Opt. Lett. **31**, 2350 (2006).
[46] Y.-F. Chen, C.-Y. Wang, S.-H. Wang, and I. A. Yu, Low-Light-Level Cross-Phase-Modulation Based on Stored Light Pulses, Phys. Rev. Lett. **96**, 043603 (2006).
[47] D. A. Braje, V. Balić, S. Goda, G. Y. Yin, and S. E. Harris, Frequency Mixing Using Electromagnetically Induced Transparency in Cold Atoms, Phys. Rev. Lett. **93**, 183601 (2004).
[48] K.-F. Chang, T.-P. Wang, C.-Y. Chen, Y.-H. Chen, Y.-S. Wang, Y.-F. Chen, Y.-C. Chen, and I. A. Yu, Low-loss high-fidelity frequency beam splitter with tunable split ratio based on electromagnetically induced transparency, Phys. Rev. Res. **3**, 013096 (2021).
[49] Y.-F. Chen, Y.-C. Liu, Z.-H. Tsai, S.-H. Wang, and I. A. Yu, Beat-note interferometer for direct phase measurement of photonic information, Phys. Rev. A **72**, 033812 (2005).
[50] S. Sevinçli, N. Henkel, C. Ates, and T. Pohl, Nonlocal Nonlinear Optics in Cold Rydberg Gases, Phys. Rev. Lett. **107**, 153001 (2011).
[51] T. Baluktsian, B. Huber, R. Löw, and T. Pfau, Evidence for Strong Van der Waals Type Rydberg-Rydberg Interaction in a Thermal Vapor, Phys. Rev. Lett. **110**, 123001 (2013).
[52] J. Sinclair, D. Angulo, N. Lupu-Gladstein, K. Bonsma-Fisher, and A. M. Steinberg, Observation of a large, resonant, cross-Kerr nonlinearity in a cold Rydberg gas, Phys. Rev. Res. **1**, 033193 (2019).
[53] N. Šibalić, J. D. Pritchard, C. S. Adams, and K. J. Weatherill, ARC: An open-source library for calculating properties of alkali Rydberg atoms, Comput. Phys. Commun. **220**, 319 (2017).